Influence of the Wavelength on Femtosecond Laser Ablation Thresholds and Incubation Coefficients of Silicon and Germanium

Javier Prada-Rodrigo[*1], Yoan Di Maio[2], Nicola Faure[1], E. Kachan[1], J.P. Colombier[1], and Xxx Sedao[1, 2]

[1] *Laboratoire Hubert Curien, UMR CNRS 5516, Université Jean Monnet, Université de Lyon, Saint-Etienne, France*
[2]*GIE Manutech-USD, 20 Rue Prof Benoit Lauras, Saint-Etienne, France*
[*]*Corresponding author's e-mail: javier.prada.rodriguo@univ-st-etienne.fr*

When using an ultrafast laser to irradiate the surface of a material, one can induce different changes in it depending on a set of laser parameters, such as the laser wavelength, laser fluence, and the total number of pulses. In our materials of interest, we are mainly concerned by two different laser-mater interaction regimes: the laser ablation regime and the sub-ablation modification regime, which are separated by the ablation threshold fluence. This fluence, depends on the laser wavelength, and the number of pulses (incubation effect). In this work, we investigated these dependencies, for mono-crystalline silicon (Si) and germanium (Ge). We measured the ablation thresholds for irradiation with 5, 10 and 50 pulses at 343, 515 and 1030 nm, for a laser pulse duration of 350 femtosecond (fs). The ablation thresholds of Si and Ge for these laser conditions are traced experimentally. The single-shot ablation thresholds for the 3 wavelengths are deduced, as well as the incubation coefficient, both of which are based on the experimental data from our study. We then discuss a number of factors which may contribute to the ablation thresholds and incubation coefficient when operating at different wavelengths.

1. Introduction

Femtosecond lasers allow for the interaction with matter in timescales faster than heat processes, resulting in a very small thermally affected area [1, 2, 3, 4]. This results in a more precise and clean machining than the one achievable with their nanosecond counterparts. Femtosecond laser ablation of semiconductors has been an area of intense fundamental and applied research for about two decades. A large amount of work has been reported on the study of dynamics and the analysis of the final state of the material [5, 6, 7, 8]. Most femtosecond ablation studies on semiconductors published to date were performed with light pulses centered around the central wavelengths of 800 and 1030 nm, respectively. Notwithstanding, recent technology development such as higher harmonic generation and optic parametric amplification has enabled femtosecond laser irradiation at a large spectrum range. The interactive steps in laser irradiation of semiconductors have been studied in near infra-red (NIR) and ultra-violet regimes (UV). Despite the large difference in photo energy of NIR and UV photons, the laser-material interaction shows similar steps, even if the absorption mechanism goes from two photon absorption to linear absorption. First, there is the generation of a free-electron plasma, then, non-thermal melting occurs, followed by, if the laser fluence (defined by the energy density of the irradiation) is sufficiently high, the ablation onset and expansion of a semi-transparent ablation layer with sharp interfaces [8].

The lowest fluence for a given number of pulses at which ablation takes place is known as the ablation threshold, and it is dependent on the laser condition and the sample's physical characteristics. Analysis of ablation and sub-ablation surface modifications of materials over a broader range of wavelengths can provide important information about the absorption processes and serve as experimental tests for advanced theoretical models [9]. In the interaction of semiconductors with femtosecond lasers there are 3 distinct regimes according to the fluence deposited: at very low fluence, the material would remain unchanged; at higher fluence, some micro-structural modification will be induced, such as amorphization [10]; at even higher fluences, ablation will take place, where the matter is ejected from the sample. It is worth mentioning that in the second regime discussed above, the underlying material is evolving on a pulse-by-pulse basis: the more laser pulses impinge on the surface the more micro-structural modifications are introduced into the material, until, at some point, the material collapses and ablation takes place, even if the laser fluence is under the single shot laser ablation threshold fluence. This effect by which the ablation threshold diminishes when irradiating with a larger number of pulses is called incubation effect [11].

Both laser ablation and incubation are of great technology importance [12, 13]. Therefore, it is worthwhile to investigate the process conditions that lead laser material interaction to undergo these routines. Laser induced mate-

rial ablation is very useful for drilling, cutting, engraving and structuring etc, whereas the subablation effects such as laser induced defects formation and/or amorphization do not entail material removal, but do cause an optic in dices modification and material properties change such as resistance to chemical etch. In particular, an application of laser induced defect formation is laser-assisted chemical etching [14, 15]. Laser-assisted selective etching is a maskless high throughput process suitable for production of high-quality complex structures, which is being widely spread since it can create structures with much higher form factor than other laser structuring techniques. To maximize the efficiency of this technique, one needs to use a laser fluence close but bellow the ablation threshold [16, 17, 18]. By precisely manipulating the laser-material interaction process, alternating amorphous-crystalline structures can be generated with almost no material removal. Following auxiliary chemical etching, highly homogeneous structures can be obtained, and the topography of the structures can be flexibly managed through precisely controlling the duration of the etching process.

Since both ablation and sub-ablation surface modification are of great interest, in this work, we investigated the influence of the pulse wavelength on the ablation threshold and the incubation coefficient of silicon (Si) and germanium (Ge). Si is extensively used in, for instance, semiconductor industry, electronics, and high-performance photovoltaics, whereas Ge is widely used as lenses and windows for thermal imaging systems. All these applications could benefit from high precision femtosecond laser micromachining of Si and Ge, such as realization of 3D microelectronic [19], device fabrication [20], and surface functionalization [21]. Therefore, in this study, we measured the ablation thresholds for 5, 10 and 50 pulses at three different wavelengths (343, 515 and 1030 nm) that are covering photon energies above and below the bandgap of Si and Ge. Then, we also studied the influence of the number of pulses in the ablation threshold. The correlation between ablation thresholds/incubation coefficients and wavelengths is sought for. The correlations of Si and Ge are compared. The difference seems to be associated with the band structures of the materials.

2. Materials and methods

The investigation was performed on 2 semiconductor materials that are commonly used in microelectronics industry: 1 mm thick silicon wafers (1 0 0) polished on both sides, and 1 mm thick high purity germanium wafers (1 0 0) polished in both sides. The surface roughness Ra of both materials is well below 1 nm. We positioned the samples using motorized XYZ translation stages from Thorlabs Inc and New Port. The control of the number of pulses and laser fluence was realized via the laser system software. The irradiation was carried out in air, at ambient conditions of temperature and pressure. Each laser irradiation condition was repeatedly used to produced multiple laser impacts and the averaged values from the measurements of these individual impacts were used for the evaluation in this report. The fluence of the pulses was calculated through dividing power measurements by the beam spot size. We measured the crater sizes with an Optical Microscope (OM) of AXIO model from Zeiss. We took the crater size as the

diameter of the area with a significant contrast change. Furthermore, for the visualization of the features beyond the OM resolution, and for the morphological inspection of the impacts on Si and Ge produced by laser irradiation, a Scanning Electron Microscope (SEM) of Jeol IT-800-SHL was used. We irradiated the samples with laser pulses centered at 1030, 515 and 343 nm wavelengths. The femtosecond laser pulses at 1030 and 515 nm were obtained from the fundamental and second harmonic of a commercial femtosecond laser system of Pharos model from Light Conversion. This laser allows for repetition rates up to 1 MHz and pulse widths varying from 100 fs to 10 ps. We selected 350 fs and a repetition rate of 50 KHz. Regarding the 343 nm pulses, we obtained them from another commercial Monaco UV laser system of Coherent Inc., that provides 343 fs pulses at the same repetition rate. All pulses were focused with f/θ lenses and the nominal focal lengths of the f/θ lenses for the different wavelengths were all identical and being 100 mm. For each wavelength, the laser fluence was adjusted using a half-wave plate (λ/2) associated with a polarizer. The pulse energy was measured with a thermopile power-meter (Gentec). The determination of the ablation threshold allows us to work in the regimes that interest us. That is why the effect in the ablation threshold of different parameters such as pulse length [10, 22] and repetition rate [23] has been studied. A widely used method for the determination of this threshold is the D^2 method [24]. It assumes a Gaussian beam and it can be expressed as eq.(1):

$$A = \frac{1}{2}A_0 \ln \frac{P}{P_{th}} \ , \tag{1}$$

where A is the ablated area, A_0 is the beam area and P and P_{th} are the irradiation power and threshold power respectively. This ablation threshold diminishes with the number of pulses due to several mechanisms grouped together in the term "incubation". Eq.(2) shows the incubation process:

$$F_{th}^N = \frac{F_{th}^1}{N^{1-S}} \to \ln F_{th}^N N = \ln F_{th}^1 + S \ln N, \tag{2}$$

here F_{th}^N and F_{th}^1 are the ablation threshold fluences (J/cm^2) for N and 1 pulses respectively, N is the number of pulses and S is the so-called incubation parameter [11]. It stands toreason that this equation must not be applicable for a very high number of pulses, since the fluence tends to zero, which is well known to be untrue. That is why some authors introduced different models taking this into account [25, 26]. However, in our case, the number of pulses we used is low enough that we can apply eq.(2).

3. Results and discussion

In this section we show first of all the morphological features, and next the determination of the ablation thresholds of Si and Ge at the 3 different laser wavelengths for 5, 10 and 50 pulses. We then use that data to calculate the single pulse ablation thresholds and incubation coefficients for each underlying material. The influence of laser wavelength on ablation and on incubation coefficient for the 2 materials is discussed, respectively.

Ablation site morphology: For each sample, the ablation thresholds were determined for a series of fixed num-

ber of pulses, as well as the different wavelengths by using the aforementioned D^2 method. SEM micrographs of some typical ablation craters on Si and on Ge are shown in Figure 1, where the area considered has been marked.
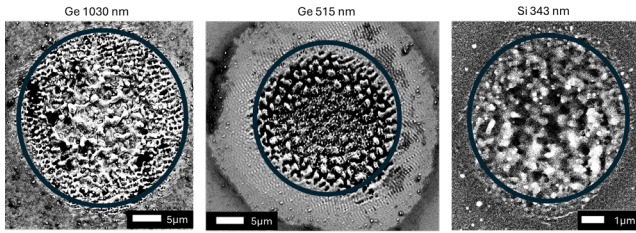

Fig. 1: SEM micrographs of Ge and Si irradiated at different laser configurations, typically, multiple shots at 1030, 515 and 343 nm central wavelengths. The blue circle represents the considered area.

One can observe from all the SEM micrographs that laser irradiation above the ablation threshold entails the formation of a circular impact, also called an ablation crater, at all wavelengths applied in this study. The circular shape of the craters is associated with the Gaussian profile of the laser beam. The size of the craters is dependent on the Gaussian beam spot size, laser pulse energy, and number of pulses used to produce these craters. It is also seen that within each impact there are various different micro- and nano structures from the centre to the peripheral area of the laser impacts. Many of these micro- and nano-structures have been reported in literature, such as Laser-Induced Periodic Surface Structures (LIPSS) within which further definitions are given to nanostructures of different scales, such as coarse LIPSS, low spatial frequency LIPSS, high spatial frequency LIPSS etc. In Figure 1, one observes clearly some of these LIPSS structures and their characteristics are clearly related to the laser wavelengths applied [28]. Notwithstanding the scientific interest, we do not investigate the LIPSS in this report but rather the surface area where the surface topography modification took place. The surface areas of the laser impacts were measured (as abovementioned multiple measures of the craters diameters were taken from identical impacts, and averaged values are used in this study), and their correlation with the laser pulse energy are studied and plotted in Figure 2.
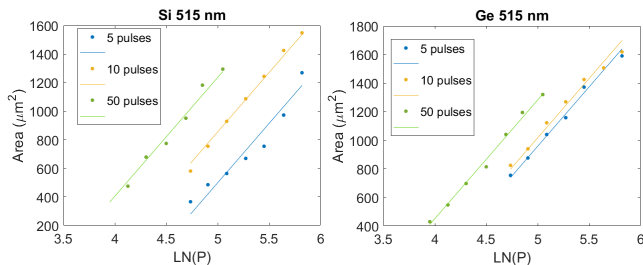

Fig. 2: Representation of the dependence of the crater size on the irradiation power for the determination of the ablation threshold at 515 nm.

Ablation thresholds: One example of the linear regressions used for this method is depicted in Figure 2, where the square powers of the craters' diameters are plotted against the natural logarithm of the laser power applied to create those craters. Both plots for Si and Ge for 515 nm

wavelength are presented in Figure 2. Furthermore, in each individual plot, one finds the data points for experiment conditions of fixed number of 5 pulses, 10 pulses, and 50 pulses. By tracking the fitting slopes and the intercepts of these data points, one derives the laser beam waist at the focal plane, as well as the ablation threshold power (from which the threshold pulse energy and threshold fluence can be calculated henceforth). Similar plots were also made for Si and Ge at 1030 and 515 nm wavelengths, but for the sake of simplicity, these are not displayed in this communication (these plots are available upon request). Nonetheless, the results of the ablation thresholds for each laser wavelength of interest are summarized in Table 1 and in Table 2, for the Si and Ge samples, respectively.

Table 1 Si ablation threshold for different number of pulses at different wavelengths.

$\lambda(nm)$	Pulses	$F_{th}(J/cm^2)$
1030	5	0.33
1030	10	0.22
1030	50	0.14
515	5	0.20
515	10	0.13
515	50	0.08
343	5	0.11
343	10	0.08
343	50	0.06

Table 2 Ge ablation threshold for different number of pulses at different wavelengths.

$\lambda(nm)$	Pulses	$F_{th}(J/cm^2)$
1030	5	0.25
1030	10	0.25
1030	50	0.20
515	5	0.10
515	10	0.10
515	50	0.08
343	5	0.15
343	10	0.09
343	50	0.07

For Si, we witness a decrease of the ablation threshold from 0.33 J/cm^2 to 0.14 J/cm^2 at laser wavelength of 1030 nm, representing a more than twofold of threshold drop when the number of pulses increased from 5 to 50. Similarly, a drop of the ablation threshold fluence at 515 nm was also observed, from 0.20 J/cm^2 down to 0.08 J/cm^2, which is also registering a more than twofold threshold value drop. Once again, at 343 nm, the ablation threshold drops from 0.11 J/cm^2 to 0.06 J/cm^2, almost two times smaller when the total pulse number shifted from 5 to 50. Concerning Ge, this tendency of ablation threshold decreasing with increas-

ing number of laser pulse still holds, at all the wavelengths. Nevertheless, we observe that the amplitude at which the ablation threshold value drops for Ge with the pulse number increase is systematically smaller than that of Si, for all the three wavelengths investigated.

Single-shot ablation threshold: In order to be able to compare our results with existing literature, and also to be able to operate our future experiment at any given number of laser pulses, for each sample and wavelength, we calculated their ablation threshold for 1 pulse (sing-shot condition) and their incubation coefficient, by using eq. (2) and by making a linear regression $(y = x + b)$ where $y = \ln(F^N_{th} N)$, $x = \ln N$, $a = S$ and $b = \ln F^1_{th}$. The linear regressions used for this method are plotted in Figure 3, and their numerical results are summarized in Table 3 and Table 4, for the Si and Ge samples, respectively.
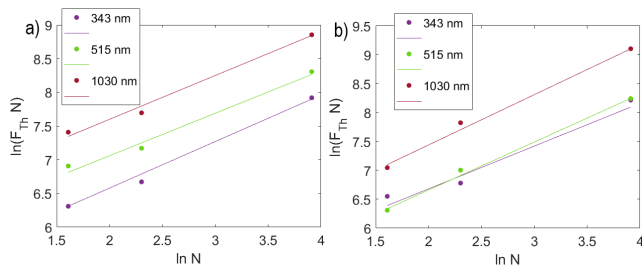

Fig. 3: Representation of the dependence of $\ln(F^N_{th} N)$, of a) Si and b) Ge with $\ln(N)$ for the calculation of their incubation coefficients and threshold fluences at 1 pulse.

We can see from Table 3 and Table 4 that, as expected, for each material, for each wavelength, the ablation threshold diminishes with the number of laser pulses applied. As for the effect of the irradiation wavelength on ablation threshold value, it is known in materials, semiconductors and dielectrics, for which there exists an energy gap between the valence and conduction band, it is necessary to supply enough energy to bridge this gap to promote valence band electrons to the conduction band. Depending on the photon energy, the absorption can be either linear or nonlinear. In each case, the result of the absorption process is the creation of free electrons in the material. As is applied to our study, the ablation threshold of Si diminishes with the wavelength of the laser, from 0.5 J/cm^2 at 1030 nm, to 0.33 J/cm^2 at 515 nm, and then to 0.18 J/cm^2 at 343 nm. As for that of Ge, it diminishes from 0.3 J/cm^2 at 1030 nm to 0.15 J/cm^2 at 515 nm. However, it does not decrease further at 343 nm wavelength. Comparing the ablation thresholds of both materials, the ones for Ge are constantly smaller than those of Si at both 1030 and 515 nm but become similar at 343 nm. We attribute such evolution to the difference in band gaps, from 1.2 eV in Si to 0.71 eV in Ge [29]. The reduction of the ablation threshold with decreasing wavelengths can be roughly explained, to a first order of approximation, by an increase in the linear absorption coefficient. To be more specific, in Si the linear absorption coefficient goes from 29.339 cm^{-1} at 1030 nm [30] to $1.4886 \cdot 10^4$ cm^{-1} at 515 nm, and then to $1.0983 \cdot 10^6$ cm^{-1} at 343 nm [31]. The small fluence threshold change from 515 nm to 343 nm, given the 70 times increase in linear absorption, points towards the importance of two-photon absorption at 515 nm. As for Ge, the coefficient goes from $1.9730 \cdot 10^4$ cm^{-1} at 1030 nm [32] to $5.9770 \cdot 10^5$ cm^{-1} at 515 nm,

and to $10.165 \cdot 10^5$ cm^{-1} at 343 nm [31]. It is clear from these data that with decreasing of the wavelength the absorption coefficient increases monotonously for Si, while for Ge this absorption is small for 1030 nm, but rather similar for 515 and 343 nm wavelengths.

The results obtained for the single pulse ablation threshold of Si at the 3 different wavelengths of interest are in good agreements to the ones in bibliography with 3 ps duration pulses for the same wavelengths [33], where ablation threshold values of 0.43, 0.22 and 0.10 J/cm^2 were published. Similar tendency was also reported for 50 ps laser pulses at these wavelengths [9]. As for the ones in Ge, we admit that we have found much less literature which is available to compare with the values we obtained through our experiments. We found nevertheless a similar result at 1030 nm central wavelength and at of pulse duration of 300 fs [34] and a similar tendency with switching wavelengths: from 800 nm and 300 fs [35], to 400 nm and 100 fs (as a side note, we assume the variation of pulse duration plays a minor role here).

Table 3 Single pulse ablation threshold and incubation coefficient of Si obtained via a linear regression applying eq. (2).

λ (nm)	F^1_{th} (J/cm^2)	S
1030	0.5 ± 0.1	0.65 ± 0.07
515	0.33 ± 0.07	0.63 ± 0.08
343	0.18 ± 0.04	0.69 ± 0.07

Table 4 Single pulse ablation threshold and incubation coefficient of Ge obtained via a linear regression applying eq. (2).

λ (nm)	F^1_{th} (J/cm^2)	S
1030	0.30 ± 0.06	0.87 ± 0.07
515	0.15 ± 0.01	0.83 ± 0.02
343	0.18 ± 0.07	0.74 ± 0.14

Incubation effect: Concerning the incubation, we observe little variation of the incubation coefficient from Table 3 and Table 4. The incubation is thought to be an interplay that is dynamically associated with laser light coupling. Therefore, the incubation effect rests on the influence of the transient temperature increase on the absorption coefficients of the sample, the transient surface morphology reduction of reflectivity, as well as a non-ablating modification of the sample material by the laser pulses in such a manner that the threshold for damage decreases [36]. This effect has been extensively studied at the surface of single-crystal metals and for dielectrics. In metal cases, incubation is related to an accumulation of energy (i.e. non-complete dissipation of the deposited energy) into plastic-strain of metal. Whereas for dielectrics the emergence of the incubation effect is closely linked to the formation of self-trapped excitons (STEs), electron-hole pairs that become bound due to Coulomb attraction. STEs can induced localized lattice rearrangements and accumulation of the defects that contribute to an increase of the material's optical absorption,

which leads to energy of subsequent laser pulses being absorbed more efficiently, ultimately leading to the reduction of the ablation threshold. Concerning semiconductors, the exact mechanisms underlying the incubation effect are not fully understood and remain a subject of ongoing research. As we mentioned earlier, the fact that the ablation threshold diminishes with increasing number of laser pulses applied per sample area suggests both materials exhibit incubation effect [37, 38], at all wavelengths examined. In terms of value, we only found some valuable information from the bibliography for it in silicon [39], in which the result for 800 nm (S=0.80) is slightly bigger than ours. We associate this smaller incubation effect to the fact that in this paper they use a repetition rate 50 times smaller than ours, giving the material more time to relax between pulses. We believe that our results spanning over the three wavelengths are novel and valuable to the community. In Table 3 and Table 4 we see that, apart from the incubation coefficient stays fairly constant with the change in wavelength for both Si and Ge, the coefficients are slightly greater in Ge than in Si, signifying a smaller importance of incubation effects. Although intriguing, we haven't been able to find any incubation study for Ge in the ultrafast laser irradiation regime. We wish our experiment data on incubation coefficient of these semiconductor materials at different laser wavelengths could shed lights and help further understanding to be achieved in future research endeavors.

4. Conclusions

Femtosecond laser ablation of Si and Ge at different harmonic wavelengths was investigated in this study. Both laser ablation thresholds and incubation coefficient of Si and Ge were sought experimentally, at 1030, 515 and 343 nm wavelengths. Experimental results reveal a decrease of the damage threshold with the wavelength, and with a dependence on the bandgap of the underlying material, bringing new data for the community in this field.

For Si, the ablation threshold values are found to decrease with the wavelength, in agreement with the existing literature. For Ge, the ablation threshold diminishes from 1030 nm to 515 nm but stays similar at 343 and 515 nm. This is qualitatively explained by taking the linear optical absorption coefficient into account. The results are found comparable to the ones in the bibliography finding similar wavelength dependency. Moreover, the incubation coefficient was also deduced for Si as well as for Ge. For a given material, the incubation coefficient remains almost invariable at different wavelengths. The incubation coefficient for Ge is slightly greater than that of Si, implying a smaller incubation behavior.

References

[1] B. N. Chichkov, C. Momma, S. Nolte, F. Von Alvensleben, and A. Tünnermann: App. Phys. A, 63, (1996) 109.

[2] E. Rebollar, M. Castillejo, and T. A. Ezquerra: Eur. Pol. J., 73, (2015) 162.

[3] R. Le Harzic, N. Huot, E. Audouard, C. Jonin, P. Laporte, S. Valette, A. Fraczkiewicz, and R. Fortunier: App. Phys. Let., 80, (2002) 3886.

[4] S. Zhang, Z. Liang, W. Hang, Z. Yang, B. Yu, and W. Wang: Nuc. Inst. and Met. in Phys. Res. B, 440, (2019) 146.

[5] N. Farid, A. Brunton, P. Rumsby, S. Monaghan, R. Duffy, P. Hurley, M. Wang, K.-L. Choy, and G. M. O'Connor: ACS Appl. Mater. Interf., 13, (2021) 37797.

[6] J.-P. Colombier, A. Rudenko, E. Silaeva, H. Zhang, X. Sedao, E. Bévillon, S. Reynaud, C. Maurice, F. Pigeon, F. Garrelie, and R. Stoian: Phys. Rev. Res., 2, (2020) 043080.

[7] S. Höhm, M. Herzlieb, A. Rosenfeld, J. Krüger, and J. Bonse: Opt. Express, 23, (2015) 61.

[8] D. Puerto, J. Solis, and J. Siegel: App. Surf. Sci., 666, (2024) 160372.

[9] A. Sikora, D. Grojo and M. Sentis: J. App. Phys., 122, (2017) 045702.

[10] J. Bonse, S. Baudach, J. Krüger, W. Kautek, and M. Lenzner: App. Phys. A, 74, (2002) 19.

[11] Y. Jee, M. F. Becker, and R. M. Walser: JOSA B, 5, (1988) 648.

[12] G. Herbst, M. Steiner, G. Marowsky, and E. Matthias: Proc. Mat. Res. Soc. Symp., Vol. 397, (1996) 69.

[13] M. Garcia-Lechuga, N. Casquero, A. Wang, D. Grojo, and J. Siegel: Adv. Opt. Mat., 9, (2021) 2100400.

[14] D. Pallarés-Aldeiturriaga, P. Roldán-Varona, L. Rodríguez-Cobo, and J. M. López-Higuera: Sensors, 20, (2020).

[15] M. Chambonneau, X. Wang, X. Yu, Q. Li, D. Chaudanson, S. Lei, and D. Grojo: Opt. Lett., 44, (2019) 1619.

[16] M. Saito and S. Kimura: AIP Adv., 7, (2017) 025018.

[17] J. Huang, L. Jiang, X. Li, A. Wang, Z. Wang, Q. Wang, J. Hu, L. Qu, T. Cui, and Y. Lu: Nanophoton., 8, (2019) 869.

[18] Y. Bellouard, A. Said, M. Dugan, and P. Bado: Opt. Express, 12, (2004) 2120.

[19] J. H. Lau: Microelec. Int., 28, (2011) 8.

[20] T. Chen, J. Si, X. Hou, S. Kanehira, K. Miura, and K. Hirao: App. Phys. Let., 93, (2008) 051112.

[21] I.S. Omeje, J. Prada-Rorigo, E. Gamet, Y. Maio, R. Guillemet, T. Itina, and X. Sedao: (in the reviewing process for this journal of laser micro- and nanoengineering)

[22] B. Lenssen and Y. Bellouard: App. Phys. Let., 101, (2012) 103503.

[23] C. S. Nathala, A. Ajami, W. Husinsky, B. Farooq, S. I. Kudryashov, A. Daskalova, I. Bliznakova, and A. Assion: App. Phys. A, 122, (2016) 1.

[24] M. Hu, J. JJ Nivas, M. Valadan, R. Fittipaldi, A. Vecchione, R. Bruzzese, C. Altucci, and S. Amoruso: App. Surf. Sci., 606, (2022) 154869.

[25] J. M. Liu: Opt. Lett., 7, (1982) 196.

[26] D. Ashkenasi, M. Lorenz, R. Stoian and A. Rosenfeld: App. Surf. Sci., 150, (1999) 101.

[27] F. D. Niso, C. Gaudiuso, T. Sibillano, F. P. Mezzapesa, A. Ancona, and P. M. Lugarà: Opt. Express, 22, (2014) 12200.

[28] D. Pallarés-Aldeiturriaga, S. Papa, A. Abou Khalil, A. Pascale-Hamri, M. Maalouf, Y. Maio, A. Guignandon, V. Dumas, and X. Sedao: App. Phys. A, 128, (2022) 100.

[29] P. Moontragoon, Z. Ikonić, and P. Harrison: Sem. Sci. and Tech, 22, (2007) 742.

[30] C. Schinke, P. Christian Peest, J. Schmidt, R. Brendel, K. Bothe, M. R. Vogt, I. Kröger, S. Winter, A. Schirmacher, S. Lim, H. T. Nguyen, and D. MacDonald: AIP Adv., 5, (2015) 67168.

[31] D. E. Aspnes and A. A. Studna: Phys. Rev. B, 27, (1983) 985.

[32] T. N. Nunley, N. S. Fernando, N. Samarasingha, J. M. Moya, C. M. Nelson, A. A. Medina, and S. Zollner: J. Vac. Sci. and Tech. B, 34, (2016) 61205.

[33] J. Thorstensen and S. E. Foss: J. App. Phys., 112, (2012) 103514.

[34] L. L. Taylor, J. Xu, M. Pomerantz, T. R. Smith, J. C. Lambropoulos, and J. Qiao: Opt. Mater. Express, 9, (2019) 4165.

[35] A. Cavalleri, C. W. Siders, C. Rose-Petruck, R. Jimenez, C. Tóth, J. A. Squier, C. P. J. Barty, K. R. Wilson, K. Sokolowski-Tinten, M. Horn von Hoegen, and D. von der Linde: Phys. Rev. B, 63, (2001) 193306.

[36] J. Bonse, S. Baudach, J. Krüger, W. Kautek, and M. Lenzner: App. Phys. A, 74, (2002) 19.

[37] P. Wang and Q. Peng: Nanotech., 35, (2023) 015401.

[38] R. Zhang, A. McDowell, F. Hegmann, R. Fedosejevs, and Y. Y. Tsui: App. Phys. A, 129, (2023) 131.

[39] C. S. R. Nathala, A. Ajami, W. Husinsky, B. Farooq, S. I. Kudryashov, A. Daskalova, I. Bliznakova, and A. Assion: App. Phys. A, 122, (2016) 2.